New broadband methods for resonance classification and high-resolution imagery of fish with swimbladders using a modified commercial broadband echosounder

Timothy K. Stanton, Dezhang Chu, J. Michael Jech, and James D. Irish

Stanton, T. K., Chu, D., Jech, J. M., and Irish, J. D. 2010. New broadband methods for resonance classification and high-resolution imagery of fish with swimbladders using a modified commercial broadband echosounder. – ICES Journal of Marine Science, 67: 365–378.

A commercial acoustic system, originally designed for seafloor applications, has been adapted for studying fish with swimbladders. The towed system contains broadband acoustic channels collectively spanning the frequency range 1.7–100 kHz, with some gaps. Using a pulse-compression technique, the range resolution of the echoes is ~20 and 3 cm in the lower and upper ranges of the frequencies, respectively, allowing high-resolution imaging of patches and resolving fish near the seafloor. Measuring the swimbladder resonance at the lower frequencies eliminates major ambiguities normally associated with the interpretation of fish echo data: (i) the resonance frequency can be used to estimate the volume of the swimbladder (inferring the size of fish), and (ii) signals at the lower frequencies do not depend strongly on the orientation of the fish. At-sea studies of Atlantic herring demonstrate the potential for routine measurements of fish size and density, with significant improvements in accuracy over traditional high-frequency narrowband echosounders. The system also detected patches of scatterers, presumably zooplankton, at the higher frequencies. New techniques for quantitative use of broadband systems are presented, including broadband calibration and relating target strength and volume-scattering strength to quantities associated with broadband signal processing.

Keywords: acoustic scattering, broadband, echosounder, fish, resonance.

Received 19 August 2008; accepted 21 October 2009; advance access publication 5 January 2010.

T. K. Stanton, D. Chu, and J. D. Irish: Department of Applied Ocean Physics and Engineering, Woods Hole Oceanographic Institution, Woods Hole, MA 02543-1053, USA. J. M. Jech: NOAA Northeast Fisheries Science Center, Woods Hole, MA 02543, USA. D. Chu: Current address: NOAA/NMFS/NWFSC/FRAMD, Montlake Blvd., East Seattle, WA 98112, USA. Correspondence to T. K. Stanton: tel: +1 508 289 2757; fax: +1 508 457 2194; e-mail: tstanton@whoi.edu.

Introduction

Acoustic echosounders have proven to be a powerful tool in studying the spatial and temporal distributions of fish. As sound can travel great distances in water, the signals can be used to probe hundreds of metres into the water, providing high-resolution images of distributions of fish. Traditionally, acoustic echosounders have operated at frequencies in the tens to hundreds of kilohertz. Two of the commonly used frequencies are 38 and 120 kHz.

A major challenge in the use of acoustic methods to study fish has been in the interpretation of echo data. Using a traditional high-frequency echosounder, the echoes depend strongly on the orientation of the fish and weakly on the frequency of the echosounder (Figure 1). These dependencies, or lack thereof, are a source of significant ambiguities when relating echoes to biologically meaningful parameters such as length and numerical density. For example, if the echoes from two patches of fish are compared with each other and if the average echo level from one is higher than that of the other, then the elevated levels could be due to (i) increase in the numerical density of fish, (ii) increase in the size of fish, (iii) a change in orientation distribution of the fish, (iv) a change in species and/or anatomical characteristics of fish, or (v) some combination of all of these. The use of ground-truthing, such as net sampling, can eliminate some of the ambiguities, but it is better to have an acoustic method with a minimum number of ambiguities, especially because it is not practical to ground-truth at every point of a survey.

The ambiguities associated with high-frequency echosounders have been addressed, in part, in earlier studies (cited below) in which the resonance frequency of the swimbladder of fish has been exploited. The resonance frequency of these fish is typically in the hundreds of hertz to low kilohertz frequencies that are much lower than the frequencies at which traditional echosounders operate (Figure 1). In the resonance region, and in contrast to the scattering at high frequencies, the scattering depends strongly on the frequency, as illustrated by the resonance peak in Figure 1. Moreover, as the frequencies are relatively low, the echoes are not strongly dependent on the orientation of the fish. As a result, the ambiguities discussed above are significantly reduced or eliminated by using frequencies that span the resonance frequency.

Swimbladder resonance can provide valuable information because the resonance frequency depends on the size and the shape of the swimbladder (Medwin and Clay, 1998). The volume of the swimbladder can be estimated through applying an acoustic-scattering model of the swimbladder to data where

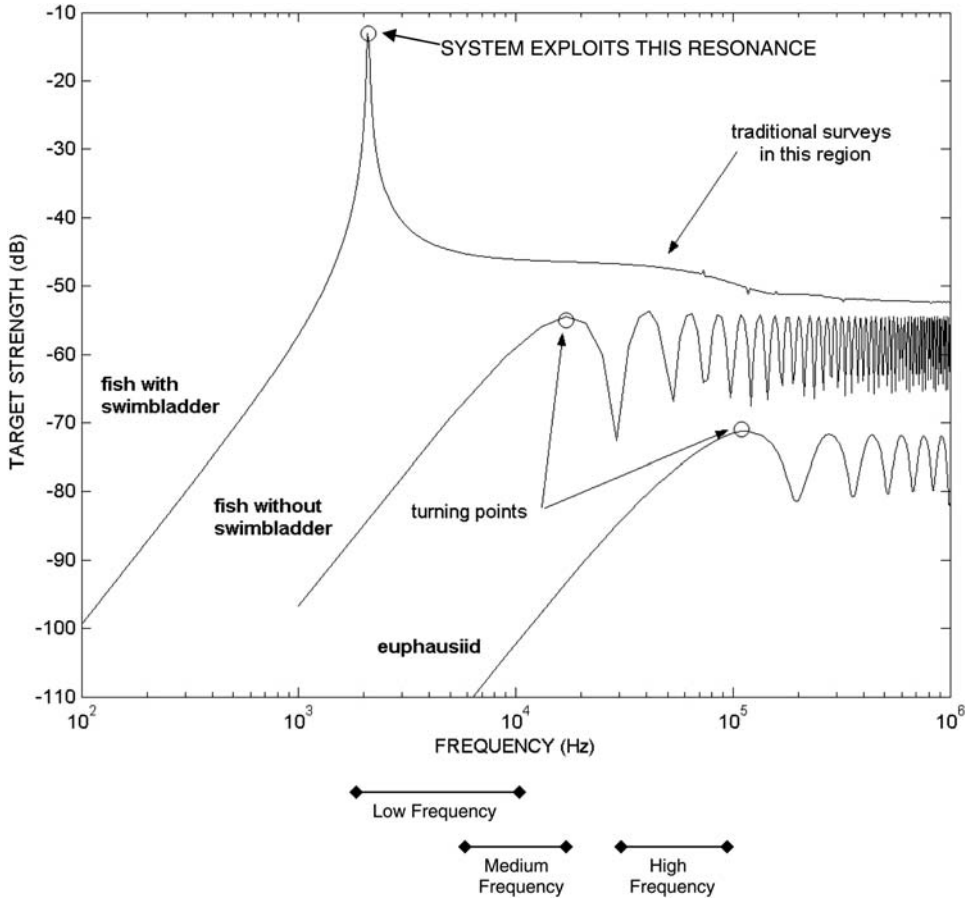

Figure 1. Frequency-dependence of backscattering by fish with swimbladders and other types of marine organism. For this simplified illustration, the fish is modelled as having a spherical swimbladder and the modal-series-based solution is used with no damping. Frequency ranges of the three acoustic channels of the Edgetech system are shown. The low-frequency channel spans the range of the resonance frequency.

the resonance is observed. The size of the fish can then, in turn, be estimated from the volume of the swimbladder, given that the size–volume and volume–depth relationships are known. As the width of the swimbladder resonance is relatively narrow, there is potential for making an estimate of the size of fish that is more accurate than with high-frequency methods. Furthermore, an assemblage of fish containing multiple sizes of fish could be characterized by observation of multiple resonances. Finally, through using such a low-frequency system, the echoes from fish with swimbladders could be distinguished easily from echoes from zooplankton and fish without swimbladders. Although the resonance classification method has many advantages, there remain challenges in the interpretation of the data. For example, the depth-dependence of the volume of the swimbladder is not well understood for at least one important species, Atlantic herring, *Clupea harengus* (Nero *et al.*, 2004). Also, it has been demonstrated for a variety of species that there is a period (12–24 h) that the swimbladder needs to adapt to a new depth (10–50 m in these studies), which results in an apparent lag in acoustic properties during vertical migration (Sand and Hawkins, 1973; Sundnes and Sand, 1975; Løvik and Hovem, 1979).

Swimbladder resonances have been observed through the measurements of transmission loss of signals in the resonance region where the signals experience excess loss as a consequence of the elevated scattering at the resonance (Weston, 1967; Diachok *et al.*, 2001; Diachok, 2002). The resonances have also been observed in the measurements of backscattering through the use of explosives (Hersey *et al.*, 1962; Chapman and Marshall, 1966; Holliday, 1972; Chapman *et al.*, 1974; Hall, 1981; Hall and Quill, 1983; Thompson and Love, 1996) and prototype hardware (Nero *et al.*, 2004). The disadvantages of explosives are quite obvious—in addition to being dangerous, it is difficult to use them frequently enough to provide continuous coverage of acoustic scattering over a large region. Furthermore, the transmission signal is not reproducible, causing difficulties in the interpretation. The disadvantage of the prototype hardware is that, by definition, it is one of a kind, not necessarily optimized for the application, and generally not accessible for use by investigators other than the inventors. Despite the disadvantages of these previous approaches, the resonances of fish with swimbladders were demonstrated to provide a strong signal, rich with information to be exploited. With these observations of swimbladder resonances, a next major step in the area is to have a commercial system in which fish can be routinely classified through the measurements of the swimbladder resonance.

The need for routine measurements of swimbladder resonance is addressed here through modification of a commercial system and development of new broadband calibration and analysis

techniques. The system, constructed by Edgetech, was originally designed for studying the seafloor with frequencies in the low kilohertz range. The lower range of the frequency band corresponds to the upper range of the resonance frequencies of common fish with swimbladders. The major modifications involved making full use of the two available (low kilohertz) broadband channels, increasing their sensitivity, and adding a third broadband channel in the 30–100 kHz range, resulting in a collective range of frequencies 1.7–100 kHz, with some gaps. Although the addition of the third channel is not necessary for fish resonance classification, it can be used to obtain higher-resolution images of fish and for detection of large zooplankton. With higher range resolution in this third channel, not only are the fish or features of the aggregation of fish resolved better, but there is potential for tilt-angle distribution to be inferred and for anatomical parts of the fish to be resolved (Stanton *et al*., 2003; Reeder *et al*., 2004).

New techniques associated with interpreting broadband echoes were also developed. The first involves calibration of a broadband echosounder with a single standard target and eliminating the source of interference that normally causes nulls in a broadband echo from a target. The general method is presented in Stanton and Chu (2008). Novel applications of the method to the three broadband channels of the Edgetech system are summarized in this paper. The second technique relates target strength (*TS*) and volume-backscattering strength (S_v) to quantities associated with broadband signal processing. The derivations of these relations are provided here for general use and in simplified form for the ocean measurements made with the Edgetech system.

The system was successfully used in a study of Atlantic herring over Georges Bank, near Cape Cod, MA, USA. Resonances of the fish were observed at ~3.7 kHz for patches of fish of varying density. By towing the system directly above the fish and through the use of pulse-compression processing, the echoes in the low kilohertz frequencies are demonstrated to have higher resolution than the corresponding echoes from a commercial 120-kHz system mounted on the ship. In addition, Rayleigh scattering was observed in the range 30–100 kHz in near-surface patches, suggesting the presence of zooplankton.

System description

Principal modifications to standard product

The system is a custom configuration of a commercial product sold by Edgetech. All modifications were performed by Edgetech. Table 1 lists major components of the system, along with their model numbers, and Table 2 summarizes the quantities associated with the three acoustic channels. The standard product is a single broadband transmitter (Shamu or 424) covering either a lower-frequency band (Shamu) or an upper frequency band (424) and whose echoes are detected by two widely spaced line arrays. The principal modification to the system was to include both transmitters so both frequency bands could be used in sequence, and to increase the number of line arrays to 14 (densely spaced) for increased receive sensitivity and better control over the beam pattern. A secondary modification was to add a broadband transducer (made by Reson) that sends and receives at a higher range of frequencies, in sequence with the other channels. Small changes to the hardware, data acquisition software, and real-time display software were made to accommodate the custom configuration.

We developed new analytical techniques and post-processing software associated with both broadband calibration and converting broadband echo data to *TS* and S_v. The resultant system spans the frequency range 1.7–100 kHz, with some gaps, with an output convertible to meaningful acoustic-scattering entities for applications such as fish. The three broadband acoustic channels will be referred to as "low frequency" (Shamu), "medium frequency" (424), and "high frequency" (Reson). Details of the system and new broadband methods are given below.

Table 1. Major hardware components of the broadband-towed system: tow body, cable, electronics, and sensors

Component	Model number
Tow body	SB-0512C
Tow cable (0.322″ double armour coax)	A320327 (Rochester)
Power/telemetry	Starmux
Shipboard computer	Discover
Chirp processor (on tow body)	FS-DW
Sidescan kit (for Reson)	Custom
Acoustic transmitter (low frequency: 1.7–10 kHz)	KT-0504 (Shamu)
Acoustic transmitter (medium frequency: 6–17 kHz)	KT-424
Acoustic transceiver (high frequency: 30–100 kHz)	TC2138 (Reson)
Hydrophone line element (1/2 m length)	HA-216
Hydrophone line element (3/4 m length)	HA-0512
Pressure sensor (for depth)	SBE-50 (Seabird)
Motion sensor (for pitch/roll)	Option, part of FS-DW

All parts are manufactured by Edgetech except where shown otherwise.

Table 2. Quantities associated with the three broadband acoustic channels

Acoustic channel	Frequency band (kHz)	Beam width (°)	Ping duration (ms)	Range resolution after pulse-compression processing (cm)
Low frequency	1.7–10	10–55	10–100	20
Medium frequency	6–17	10–25	10–100	10
High frequency	30–100	7–23	2–10	3

Beam widths are for the transceive mode for the low- and medium-frequency channels, and receive mode for the high-frequency channel. The transmit beam width for the high-frequency (transceiver) channel is the same as the receive beam width. The frequency bands correspond to a range of usable energy rather than the traditional definition involving −3 dB values.

Hardware

The system consists of a tow body, shipboard electronics, and a tow cable (Figures 2 and 3). The tow body contains the transducers, pitch-and-roll sensors, a depth sensor, and electronics. The shipboard electronics are used to control the electronics on the tow body (such as sending trigger commands) and to receive, store, and display data in real time. In addition to being used for towing the tow body, the cable also provides power to the electronics and provides a means for two-way communication between the shipboard electronics and electronics on the tow body for control and data telemetry.

There are three acoustic channels, all broadband. The low- and medium-frequency channels involve acoustic transmitters and a receive array, and the high-frequency channel involves a single

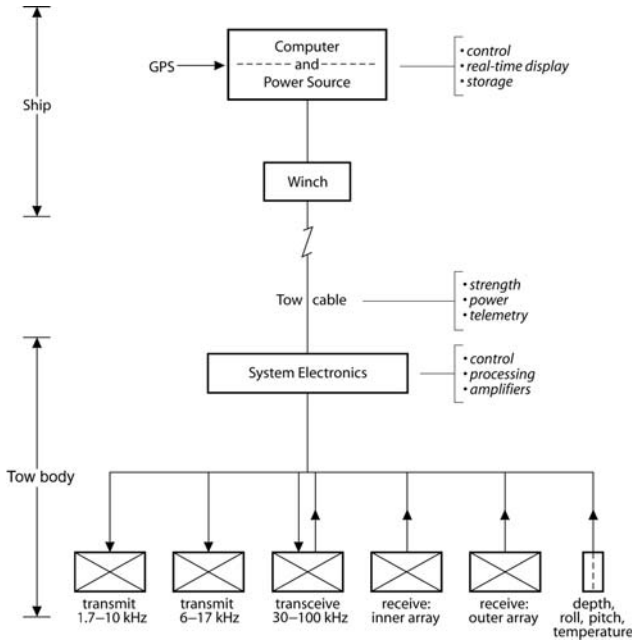

Figure 2. Block diagram of sensor channels of the Edgetech system. The three broadband acoustic channels are shown along with the channels associated with the pitch, roll, temperature, and depth sensors. There are electronics on both the tow body and the ship. Transmitter, receiver, and processing electronics for the acoustic channels are on the tow body, whereas the shipboard electronics include a power supply and computer for control, as well as for storage and display of data.

transducer that both sends and receives sound. The two transmitters and one transceiver transducer are in the nose of the tow body, and the array fills most of the flat portion of the tow body in the tail section (Figure 3b). The transmitters use the standard transmit channels that had normally been provided by Edgetech, and the transceiver transducer uses electronics, also provided by Edgetech, originally designed for sidescan applications.

The receive array consists of 14 line arrays (Figure 3b). The line arrays are spaced so as to reduce sidelobes in the beam pattern, as described below. In addition, the line arrays are divided into an inner array of six line arrays (all parallel to each other), and an outer array of eight line arrays (two per side). This division helps to address, crudely, the fact that the width of the main lobe of the beam patterns depends inversely on acoustic frequency. As the frequencies span a large range, the beam patterns vary accordingly. Ideally, there should be a constant beam-width array. However, for practical reasons, the division is used—the low-frequency band receives echoes from all 14 line arrays (inner + outer arrays), and the medium-frequency band receives echoes from only the inner six line arrays.

Transmit signals, pulse-compression processing, and display of data

The system is programmable, making its use adaptable to a wide range of applications. Specifically, the transmit signals, receiver gains, and triggering sequence are separately programmable. The transmit signals can be programmed either through the use of an equation for linear-frequency modulation (chirp) or through loading a binary file with a waveform. Using the equation, the amplitude, the duration of the signal, and the range of frequencies in the chirp can be specified. The rate at which the signals are transmitted is also programmed (including simultaneous or sequential transmissions).

As broadband transducers are not strongly resonant at any particular frequency, they are inherently insensitive. This is compensated for through the use of long broadband signals and signal processing of the echoes that optimize their use. The signal used in this case is the commonly used chirp signal (although there are other classes of signals available). Here, the range of frequencies of the band is applied uniformly to the transmitter through a gradual sweep across the band (Figure 4a and b).

Processing of the broadband echoes involves pulse-compression processing:

$$\mathrm{cp}_r(t) = k_{\mathrm{cp}} v_r(t) \otimes v_{\mathrm{rep}}(t), \tag{1}$$

where

$$k_{\mathrm{cp}} \equiv R_{\mathrm{rep}}^{-1}(0), \tag{2}$$

and

$$R_{\mathrm{rep}}(t) \equiv v_{\mathrm{rep}}(t) \otimes v_{\mathrm{rep}}(t). \tag{3}$$

Here, the compressed-pulse signal, $\mathrm{cp}_r(t)$, is the cross correlation ($\otimes$) between the echo voltage, $v_r(t)$, and a replica signal, $v_{\mathrm{rep}}(t)$. Usually, the voltage applied to the transmitter was used as the replica. The term k_{cp} is a normalization factor. This processing is based on matched filter processing, but because the scattering characteristics of the scatterers (fish in this case) are not known *a priori*, a replica waveform (in place of the transmit waveform) cannot be determined for optimum processing (Turin, 1960). This type of processing is prevalent throughout radar and sonar applications, including one narrowband and one broadband commercial echosounder for studying fish and zooplankton in the ocean (Ehrenberg and Torkelson, 2000; Ross and Lawson, 2009), and various laboratory applications with zooplankton, fish, and squid (Chu and Stanton, 1998; Reeder *et al.*, 2004; Au and Benoit-Bird, 2008; Lee *et al.*, 2009).

For the ideal case in which the scattering and system response are independent of frequency across the band, the duration of the compressed-pulse signal is approximately equal to the inverse bandwidth of the original signal applied to the transducer (Figure 4c). Also, the improvement in the signal-to-noise ratio of the processed signal is approximately directly proportional to the bandwidth.

For realistic targets and system response, the above relations still hold, but with degradation. Nonetheless, there is significant improvement in the signal, both with respect to range resolution of the signal and signal-to-noise ratio. For example, the transmit signal in the low-frequency channel had a spectrum that was 14 kHz wide and spanned beyond the lower and upper edges of the response of the transmitting transducer. Although the usable spectrum of the transmitter was ~10 kHz, the response was strongest in a 5-kHz band. As a result, most of the signal in the water after passing through the transducer was ~5-ms long (vs. the 10-ms-long applied signal) with a bandwidth of ~5 kHz. The range resolution of the 5-ms-long signal, unprocessed, is ~4 m. Once processed, the width of the autocorrelation function is

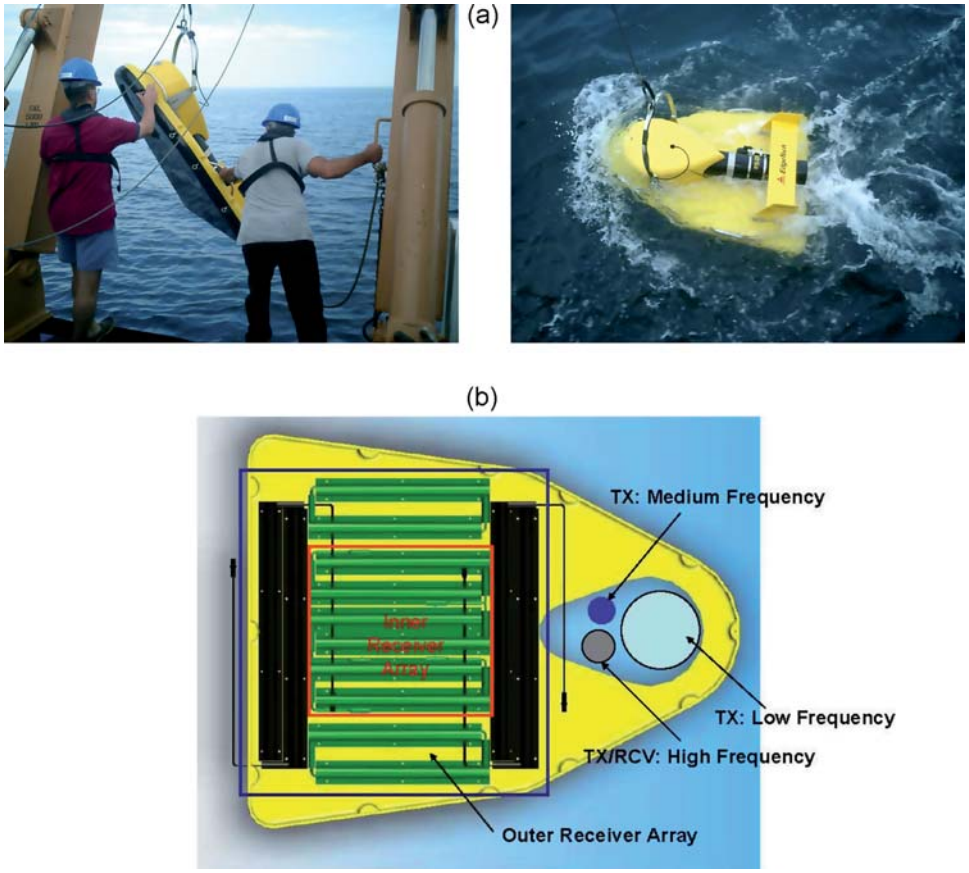

Figure 3. (a) Edgetech tow body at deployment. (b) An illustration of the underside of the tow body based on its mechanical drawing. The transmitting transducers for the low- and medium-frequency channels are in the nose of the tow body along with the transceiver transducer for the high-frequency channel. The inner array of line hydrophones receives the acoustic echoes for the medium-frequency channel, and the entire array (inner plus outer) receives echoes for the low-frequency channel.

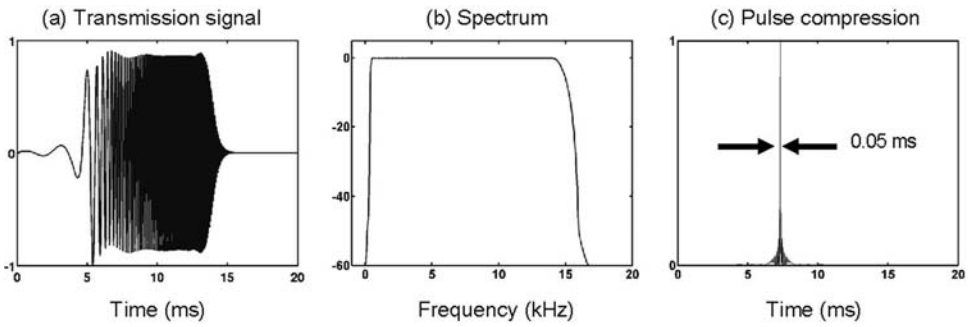

Figure 4. Linear-frequency-modulated, or chirp, signal. (a) Raw waveform, as applied to the transducers. (b) Frequency spectrum of signal. (c) Envelope of autocorrelation function (pulse-compression or matched filter processing) of the signal. The width of the main lobe of the autocorrelation function is approximately equal to the inverse bandwidth of the signal. Therefore, for a signal 10 ms long in the left panel with ~14 kHz bandwidth, the width of the main lobe of the compressed-pulse signal in the right panel is ~0.05 ms.

~0.25 ms, giving a range resolution of ~20 cm. The autocorrelation function here is from the cross correlation with the echo due to a perfectly reflecting interface with uniform frequency response. Non-uniform scattering properties of the scatterer will further degrade performance.

The echoes are processed using Equations (1)–(3) in real time in the electronics contained within the tow body. Both the compressed-pulse signals and raw unprocessed signals are telemetered in digital form through the tow cable to the shipboard computer for real-time display and storage. The echograms of the compressed-pulse signals from each of the three channels are displayed while, at the same time, those signals and the raw signals are stored for future use. In addition to the acoustic-scattering data, other data such as pitch, roll, and depth of the tow body are displayed and stored.

Beam-pattern design

The beam patterns of the low- and medium-frequency channels were designed through the choice of the spatial configuration of the receiver line arrays. The beam pattern of the high-frequency channel was determined by the diameter of the single transducer that was used to transmit and receive the echoes. There was only one diameter available from the manufacturer for this transducer.

The beam patterns of the low- and medium-frequency channels were designed so that the main lobes of the beams would be close to conical and the side lobes relatively low. A common method for controlling side lobes is through spatially shading the amplitude of the gains of the elements (e.g. gain of element decreasing with increasing distance from the centre of the array). However, along with that shading comes a loss of sensitivity (which is proportional to the sum of the gains). Therefore, a method was chosen in which the gain was uniform and the separation between the elements was varied so that their spacing was non-uniform. This latter approach maximizes the sensitivity while reducing the side lobes. A Chebychev spacing was used. Simulations of beam patterns using this spacing show that over the range of frequencies, the maximum value of side lobes is roughly 20 and 14 dB below the maximum value of the main lobe for the low- and medium-frequency channels, respectively. The higher side lobes in the latter case are presumably attributable to the fact that this channel involves fewer array elements and a coarser spacing relative to the acoustic wavelength.

Calibration

Calibration of the system is a complex task. There are significant challenges associated with the fact that each channel is broadband, the sensitivity of transducers can depend on depth, and each transducer creates a single beam whose width is frequency-dependent. A standard target (sphere) approach was used to provide system response as a function of frequency, angle, and depth. The system was calibrated against depth by suspending a sphere below the system and measuring echoes from the sphere every 10 m from the surface down to the deepest depth required (180 m in this case). Challenges associated with scattering resonances of the sphere and the limitations associated with the transducers generating single (not split or multi-) beams were addressed through two new methods, described below.

The system was calibrated under various conditions and at several locations at sea. The first at-sea calibrations took place over Georges Bank off of Cape Cod, MA, during the period 7–15 September 2005 on the FRV "Delaware II", at the site of the studies of Atlantic herring. Subsequent calibrations took place off of Provincetown, Cape Cod, MA, on 11 September and 9 October 2006, using the RV "Tioga".

Types of sphere

Given the wide range of frequencies, a correspondingly wide range of diameters of spheres was studied for calibrating the system. The smaller spheres studied were solid elastic, but for larger diameters, a solid material was not used because of its excessive weight. In this latter case, two types of sphere were studied, air- and water-filled spherical elastic shells. The focus of the studies was to design a combination of sphere and signal-processing analysis to minimize the effects of resonances from the sphere. For the high-frequency channel, an air-filled aluminium spherical shell, 41.5 cm in diameter, was used. Data were analysed using a partial-wave analysis that exploits the echo from the front interface alone and is relatively independent of frequency. For the low- and medium-frequency channels, a 20-cm-diameter solid aluminium sphere was used. A full-wave analysis was used for the medium-frequency channel, because the resonances were not strong in this region and the partial waves were difficult to resolve. Owing to noise issues, a partial-wave analysis was used for the low-frequency channel. Details of these analyses are summarized below.

Location of sphere in single beam

As this system did not have split- or multibeam capabilities, the location of the sphere in the (single) beam needed to be determined through a novel method. The location of the sphere in the beam was inferred through a combination of echo level and pitch-and-roll data concerning the tow body. The measurements were designed with the idealized goal of the sphere being suspended directly below the tow body which, in turn, was suspended directly below the ship. Lines were tied to the tow body from the termination point of the tow cable to constrain it to remain horizontal with the intention of the centre of the main lobe being directly aimed at the sphere. Under these ideal conditions, there would be no beam-pattern effects in the data. However, because of the normal conditions of the at-sea experiments, there were significant deviations from the goal which needed to be accounted for. The best conditions involved the ship being anchored. Under such conditions, the suspension cable for the tow body was vertical. However, as the ship still rolled and pitched in the waves, the wire moved up and down, causing the tow body to pitch and roll, as indicated by the data from the pitch-and-roll sensors. Under conditions where the ship was not anchored, there was the added complication of the cable angle not being vertical because the ship was drifting.

The motion of the tow body was accounted for through examining plots of echo level as a function of roll-and-pitch angle of the tow body. Selection of the pings was based on combined criteria of high echo level and being within a narrowly defined range of roll-and-pitch angles, each near 0°. The analysis was based on the assumption that those highest echoes within the narrow range of roll-and-pitch angles were associated with the sphere being in the centre of the main lobe of the beam. Normally, at least 200 echoes were analysed, which appeared to provide an adequate number of echoes from the centre of the beam.

Beam patterns

Information on the beam pattern was extracted from calibration data collected at sea at the operational depth through an indirect method. Most of the motion of the tow body involved pitch because of the configuration of the tow bridle and the fact that the tow body was designed to move forward. Therefore, the combination of the up-and-down motion of the tow cable and drift of the ship (when not anchored) led mostly to pitch motion. This constraint of motion (pitch only) fortuitously allowed the use of the calibration data to estimate the beam patterns of the system in the vertical plane. To do so, the pitch angle of the tow body is set equal to the beam angle, with an offset. The pitch angle of the tow body was sampled at 8 Hz, and the angle measured closest in time to a received echo was used in association with that echo to construct the beam pattern. The offset is because the tow cable was not vertical and it needed to be determined empirically from the echo data with the assumption that the strongest echoes were from the centre of the beam. The beam-pattern

data were reasonably consistent with the predictions, both with respect to width of the main lobe, overall side-lobe levels (but not precise structure), and across the band of frequencies of each acoustic channel.

Partial- and full-wave scattering analysis

With greater than an octave bandwidth per channel, the use of a standard target posed a challenge. The scattering by targets such as spheres contains strong resonances at many frequencies, and the spectral separation between those resonances is much smaller than one octave. These resonances are avoided in narrowband systems by designing the sphere so that the acoustic frequency is between resonances. However, with a broadband system, the frequencies may span multiple resonances, which can degrade the calibration significantly. Several approaches were explored and new methods developed to address this problem. For the cases in which the resonances were the strongest, a partial-wave analysis was developed in which a combination of signal processing and scattering physics was used to remove the resonance effects completely, leaving a scattered signal that varies only slightly with frequency (Stanton and Chu, 2008). For cases where the resonances were weak, then a full-wave analysis was sometimes used.

The partial-wave analysis works on the principle that the scattering by a sphere is attributable to a number of scattering processes; involving an echo from the front interface, internally refracted waves, and circumferential waves. These partial waves arrive at the receiver at different times. The partial-wave echo from the front interface alone is relatively independent of frequency, whereas the sum of all partial waves (the full wave) has significant resonances because of the interference between the various partial waves. With the standard calibration spheres used in fisheries acoustics, narrowband acoustic systems cannot resolve these waves, so they measure the full wave. As the full wave potentially can experience significant resonance effects attributable to interference between the partial waves, the sphere must be designed so that the system frequency is between the resonances and these effects minimized. For a broadband system, this full-wave approach may not work satisfactorily because the broadband signal spans multiple resonances. However, a broadband system, especially through the use of pulse-compression processing, can resolve more readily the partial waves and eliminate the interference problem. It is especially desirable for the broadband signal to resolve the echo from the front interface, which is not strongly dependent on frequency. In that case, calibration would not be prone to the errors associated with uncertainties in the prediction of locations of the narrow resonances.

The system response $H(\omega)$ of a broadband channel has been derived by Stanton and Chu (2008) in terms of the pulse-compression signals given in Equation (1) and the scattering physics of the target (ω is the angular frequency). Accounting for the scattering physics included convolving the impulse response of the exact solution to the scattering by the sphere, with the voltage applied to the transmitting transducer. Spreading and absorption effects are accounted for in the equation so that $H(\omega)$ reflects solely the combined efficiencies of the transmitting (voltage-to-pressure) transducer and the receiving (pressure-to-voltage) transducer.

The expression derived by Stanton and Chu (2008) is general in that it can accommodate either a partial- or a full-wave analysis. Specifically, through temporal gating, one can choose whether or not to select the echo from the front interface only, or all partial waves. Once the selection is made, the appropriate predicted waveform (single partial wave or full wave) is used through calculating the impulse response of the scattering. In short, the (gated) predictions of the partial- or full-wave waveforms used in Equation (1) are matched with the corresponding (gated) waveform selected in the measurement.

For the broadband three-channel system described here, a combination of types of sphere and approach was used. If one were to apply the standard full-wave analysis for the high-frequency channel, the sphere would need to be very small (and hence, not practical) for the scattering to be void of significant resonances. Instead, a large, air-filled spherical aluminium shell, 41.5 cm in diameter, was used in combination with a partial-wave analysis. Comparing this approach with a full-wave analysis where the resonances were averaged across frequencies showed a reduction in error (through the use of a partial-wave analysis) associated with the resonances of $\sim$3 dB.

For the low- and medium-frequency channels, a solid aluminium sphere, 20 cm in diameter, was principally used. For this combination of frequencies and diameter, the resonances were weak, allowing for the possibility of either a full- or a partial-wave analysis. As the partial-wave returns were relatively close to each other in the medium-frequency channel, a full-wave analysis was used. However, the low-frequency channel posed a greater problem because there was noise contaminating the signal. To eliminate some of the noise, a partial-wave analysis was used (i.e. echo from the front interface only). Although some error may exist by potentially including a portion of an unwanted partial wave, the noise was greater than any partial wave that immediately followed the echo from the front interface. Hence, the greatest source of error in this case was system noise (which was smaller than the echo from the front interface).

Below 2.5 kHz, the signal-to-noise ratio of the sphere echo was unacceptable, and the echoes from flat sections of the seafloor were used to estimate the sensitivity of the low-frequency channel. Sections of seafloor were chosen where there were no apparent echoes from below the seafloor and where the echoes were consistent from ping to ping. The frequency response of the seafloor echo was assumed, as an approximation, to be constant over the band 1.7–2.5 kHz. The spectrum of the seafloor echo was then adjusted so that its level matched that of the known echo from the sphere at 2.5 kHz.

Depth-dependence of the system response

The studies showed that the high-frequency transducer, which was designed for the tested range of depths, was insensitive to depth across its entire frequency band. In contrast, the sensitivity of the low- and medium-frequency channels depended strongly on depth (up to 5 dB variation for portions of the response of each of the two channels). The system response for the low- and medium-frequency channels, which appeared to have resonance properties near the surface, tended to flatten out at the greater depths, especially for the low-frequency channel. This observation is most likely because of compression of the cork backing of these transducers and causing, in essence, a mechanical "short", and eliminating the stronger resonance.

Equations for post-processing broadband data: *TS* and S_v

To determine *TS* and S_v from the pulse-compressed broadband echoes, the equations normally associated with those quantities

are re-derived in terms of the broadband signal-processing operations. As these equations relating broadband processing to *TS* and S_v are being presented for the first time and are of general applicability, derivations of the equations are summarized briefly. The derivations use the equations presented in Stanton and Chu (2008), where the system response of a broadband system is derived from measurements from a calibration sphere. The equations use the same notation and definitions as in that paper. Derivations concerning *TS* and S_v are first given for each quantity for a more general case, then a simplified form is given pertaining to our specific approach.

Target strength

The *TS* of the target of interest (fish or zooplankton in this case) is defined in terms of the differential backscattering cross section $\sigma_{\mathrm{bs}}^{(\mathrm{tar})}$:

$$TS^{(\mathrm{tar})} = 10\log\sigma_{\mathrm{bs}}^{(\mathrm{tar})} \tag{4}$$

and

$$TS^{(\mathrm{tar})} = 10\log\left|F_{\mathrm{bs}}^{(\mathrm{tar})}(\omega)\right|^2, \tag{5}$$

where $\sigma_{\mathrm{bs}}^{(\mathrm{tar})}$ is equal to the square of the magnitude of the backscattering amplitude $F_{\mathrm{bs}}^{(\mathrm{tar})}(\omega)$.

Equations (1)–(5) of Stanton and Chu (2008) were derived to relate the scattering amplitude $F_{\mathrm{bs}}^{(\mathrm{cal})}(\omega)$ of the calibration sphere to system response and other quantities. Those equations can be applied to this problem by replacing the superscript (cal) with the superscript (tar), which denotes the association of the quantities with the target measurement. With that substitution, the backscattering amplitude of the target of interest is

$$F_{\mathrm{bs}}^{(\mathrm{tar})}(\omega) = \frac{V_r^{(\mathrm{tar})}(\omega)}{V_t^{(\mathrm{tar})}(\omega)H(\omega)L^{(\mathrm{tar})}(\omega)}, \tag{6}$$

where $V_r^{(\mathrm{tar})}(\omega)$, $V_t^{(\mathrm{tar})}(\omega)$, and $L^{(\mathrm{tar})}(\omega)$ are the voltage received as a result of the echo from the target, the voltage applied to the transmitter, and the two-way transmission loss (on a linear scale) associated with the target measurement, respectively.

Multiplying the numerator and denominator of this expression by the complex conjugate (denoted by *) of the replica $V_{\mathrm{rep}}^{(\mathrm{tar})*}(\omega)$ and using Equation (8) of Stanton and Chu (2008), which relates the compressed-pulse signal to voltages in the frequency domain, yields an expression for the backscattering amplitude in terms of the compressed-pulse signals:

$$F_{\mathrm{bs}}^{(\mathrm{tar})}(\omega) = \frac{\mathrm{CP}_r^{(\mathrm{tar})*}(\omega)}{L^{(\mathrm{tar})}(\omega)H(\omega)\mathrm{CP}_t^{(\mathrm{tar})*}(\omega)}, \tag{7}$$

where $\mathrm{CP}_r^{(\mathrm{tar})}(\omega)$ and $\mathrm{CP}_t^{(\mathrm{tar})}(\omega)$ are the Fourier transforms of the compressed-pulse signals $\mathrm{cp}_r^{(\mathrm{tar})}(t)$ and $\mathrm{cp}_t^{(\mathrm{tar})}(t)$, respectively, as defined below:

$$\mathrm{cp}_r^{(\mathrm{tar})}(t) \equiv k_{\mathrm{cp}}^{(\mathrm{tar})} v_r^{(\mathrm{tar})}(t) \otimes v_{\mathrm{rep}}^{(\mathrm{tar})}(t) \tag{8}$$

and

$$\mathrm{cp}_t^{(\mathrm{tar})}(t) \equiv k_{\mathrm{cp}}^{(\mathrm{tar})} v_t^{(\mathrm{tar})}(t) \otimes v_{\mathrm{rep}}^{(\mathrm{tar})}(t). \tag{9}$$

Here, $\mathrm{cp}_r^{(\mathrm{tar})}(t)$ is the compressed pulse associated with the measurement of the target of interest in which the received voltage attributable to the backscattering by the target is cross correlated with the replica signal $v_{\mathrm{rep}}^{(\mathrm{tar})}(t)$. Similarly, the second term, $\mathrm{cp}_t^{(\mathrm{tar})}(t)$ is the compressed pulse calculated by cross correlating the applied voltage used in that measurement with the replica signal. The normalization constant, $k_{\mathrm{cp}}^{(\mathrm{tar})}$, which is defined in Equation (2) [the reciprocal of the autocorrelation function of $v_{\mathrm{rep}}^{(\mathrm{tar})}(t)$ evaluated at $t = 0$] is the same for each compressed-pulse signal in Equation (7) and cancels out (implicitly), because it appears as a factor to both the numerator and the denominator. The standard notation convention lower case cp for the time domain and upper case CP for the corresponding quantity in the frequency domain is followed.

Inserting the expression for $H(\omega)$ from Equation (9) of Stanton and Chu (2008) into Equation (7) above gives

$$F_{\mathrm{bs}}^{(\mathrm{tar})}(\omega) = \frac{\mathrm{CP}_r^{(\mathrm{tar})*}(\omega)}{\mathrm{CP}_r^{(\mathrm{cal})*}(\omega)} \frac{L^{(\mathrm{cal})}(\omega)}{L^{(\mathrm{tar})}(\omega)} \frac{\mathrm{CP}_{\mathrm{pred}}^{(\mathrm{conv})*}(\omega)}{\mathrm{CP}_t^{(\mathrm{tar})*}(\omega)}, \tag{10}$$

where $\mathrm{CP}_r^{(\mathrm{cal})}(\omega)$ is the Fourier transform of the compressed-pulse echo received from the calibration sphere, $L^{(\mathrm{cal})}(\omega)$ is the two-way propagation loss (on a linear scale) attributable to spherical spreading and absorption between the transceiver and the calibration sphere, and $CP_{\mathrm{pred}}^{(\mathrm{conv})}(\omega)$ is the Fourier transform of the cross correlation between the replica signal used in the calibration measurement and the convolution of the impulse response of the predicted echo from the calibration sphere and transmit signal used in the calibration measurement (Stanton and Chu, 2008). Equation (10) represents the case where the angle at which the target in the beam corresponds to the same angle at which the calibration sphere is in the beam.

Equation (10) can be simplified if the transmit and replica signals used in the calibration measurement are the same as the corresponding quantities in the target measurement:

$$F_{\mathrm{bs}}^{(\mathrm{tar})}(\omega) = \frac{\mathrm{CP}_r^{(\mathrm{tar})*}(\omega)}{\mathrm{CP}_r^{(\mathrm{cal})*}(\omega)} \frac{L^{(\mathrm{cal})}(\omega)}{L^{(\mathrm{tar})}(\omega)} F_{\mathrm{bs}}^{(\mathrm{pred})}(\omega), \tag{11}$$

where $F_{\mathrm{bs}}^{(\mathrm{pred})}(\omega)$ is the predicted scattering amplitude of the calibration sphere. Equation (10) or (11) can be used with either a partial- or a full-wave calibration method. It is important that the processing gate used in calculating $F_{\mathrm{bs}}^{(\mathrm{pred})}(\omega)$, which appears explicitly in Equation (11) and implicitly in Equation (10), be the same as that used in the calibration measurement. Details of the procedure are given in Stanton and Chu (2008).

Volume-backscattering strength

The volume-backscattering strength S_v is defined in terms of the volume-backscattering coefficient s_v:

$$S_v = 10\log s_v. \tag{12}$$

Calculation of s_v involves averaging the echoes from multiple targets randomly located in the acoustic beam over a number of statistically independent pings. An element of the calculation is equivalent to integrating the square of the echo for the duration of the time gate and is commonly referred to as echo integration. Below, equations for s_v are derived for pulse-compression processing of broadband signals.

For the case of echoes from the volume of multiple targets received and processed through pulse-compressed processing, the resultant signal, $\mathrm{cp}_{r,j}^{(\mathrm{vol})}(t)$, for the jth ping is

$$\mathrm{cp}_{r,j}^{(\mathrm{vol})}(t) = k_{\mathrm{cp}}^{(\mathrm{vol})} v_{r,j}^{(\mathrm{vol})}(t) \otimes v_{\mathrm{rep}}^{(\mathrm{vol})}(t), \tag{13}$$

where $v_{r,j}^{(\mathrm{vol})}(t) = \sum_i v_{r\_i,j}^{(\mathrm{tar})}(t)$, $v_{r\_i,j}^{(\mathrm{tar})}(t)$ is the voltage measured attributable to the echo from the ith target of interest (randomly located in the beam) in the jth ping, and $k_{\mathrm{cp}}^{(\mathrm{vol})}$ is the normalization constant calculated in terms of the replica signal $v_{\mathrm{rep}}^{(\mathrm{vol})}(t)$ used in the volume-scattering measurements.

The Fourier transform of the above expression gives the compressed-pulse signal in the frequency domain:

$$\mathrm{CP}_{r,j}^{(\mathrm{vol})}(\omega) = k_{\mathrm{cp}}^{(\mathrm{vol})} V_{r,j}^{(\mathrm{vol})*}(\omega) V_{\mathrm{rep}}^{(\mathrm{vol})}(\omega), \tag{14}$$

where $V_{r,j}^{(\mathrm{vol})*}(\omega) = \sum_i V_{r\_i,j}^{(\mathrm{tar})*}(\omega)$, and $V_{r,j}^{(\mathrm{vol})}(\omega)$ and $V_{\mathrm{rep}}^{(\mathrm{vol})}(\omega)$ are the Fourier transforms of $v_{r,j}^{(\mathrm{vol})}(t)$ and $v_{\mathrm{rep}}^{(\mathrm{vol})}(t)$, respectively. Choice of the window within which the Fourier transform is calculated is important. In this application, the duration T of the Fourier-transform window is set equal to the duration of the echo-integration gate, which is chosen to be much longer than the duration of the compressed-pulse signal from a given target, or, equivalently, the duration of the echo-integration processing is much longer than the inverse bandwidth of the broadband signal.

As each frequency component of the echoes from the individual targets is assumed to have a phase that is randomly and uniformly distributed over the full range $0-2\pi$, then the mean-square echo can be calculated through the average of the squared echoes of all individual targets within the processing gate and for all pings of interest (i.e. averaging across the index j) at each given frequency. In terms of the processing, this averaging corresponds to the average of the echo-integration values calculated in the processing gate described above. To relate the mean-square echo to quantities associated with the scatterers, the formulation needs to take into account the beam-pattern effects. For narrowband signals and traditional signal processing (i.e. no pulse-compression processing), this has been considered in earlier works and is summarized in Medwin and Clay (1998). In essence, the summation in the average is converted into an integral and the result is expressed in terms of the effective insonified volume $V(\omega)$ and the associated integral $\Psi_D(\omega)$ (or equivalent beam angle) of the square of the transceiver beam pattern:

$$V(\omega) = \frac{1}{2} c T r_{\mathrm{vol}}^2 \Psi_D(\omega), \tag{15}$$

where

$$\Psi_D(\omega) \equiv \int\int B_r^2(\omega) B_t^2(\omega) \mathrm{d}\Omega, \tag{16}$$

c is the speed of sound, r_{vol} the distance to the scatterers, B_r and B_t the receive and transmit beam patterns, respectively, and Ω the solid angle. To perform the integral over the beam pattern, the system response was separated into the product of the response in the centre of the main lobe of each beam pattern and the beam patterns themselves, which are normalized to the response at the centre of the main lobe (the main lobes of the transmitter and receiver are assumed to have the same centre).

After averaging the echoes over many statistically independent pings, the volume-backscattering coefficient is

$$s_v(\omega) = \frac{\left\langle \left| CP_{r,j}^{(\mathrm{vol})}(\omega) \right|^2 \right\rangle \left| L^{(\mathrm{cal})}(\omega) \right|^2}{\left| CP_{r\_0}^{(\mathrm{cal})}(\omega) \right|^2 \left| L^{(\mathrm{vol})}(\omega) \right|^2} \frac{\left| CP_{\mathrm{pred}}^{(\mathrm{conv})}(\omega) \right|^2}{k_{cp}^{(\mathrm{vol})^2} \left| V_t^{(\mathrm{vol})}(\omega) \right|^2 \left| V_{\mathrm{rep}}^{(\mathrm{vol})}(\omega) \right|^2 V(\omega)}, \tag{17}$$

where $\langle \cdots \rangle$ denote the average over many statistically independent pings (i.e. an average over all j), $\mathrm{CP}_{r\_0}^{(\mathrm{cal})}(\omega)$ corresponds to the calibration measurement where the calibration sphere is in the centre (maximum response) of the beam, $L^{(\mathrm{vol})}(\omega)$ corresponds to the two-way propagation loss to the scattering volume, and $V_t^{(\mathrm{vol})}(\omega)$ is the Fourier transform of the transmit signal in the volume-scattering measurement.

Equation (17) can be simplified if the transmit and replica signals used in the calibration measurement are the same as the corresponding quantities in the volume-scattering measurement:

$$s_v(\omega) = \frac{\left\langle \left| \mathrm{CP}_{r,j}^{(\mathrm{vol})}(\omega) \right|^2 \right\rangle}{\left| \mathrm{CP}_{r\_0}^{(\mathrm{cal})}(\omega) \right|^2} \frac{\left| L^{(\mathrm{cal})}(\omega) \right|^2}{\left| L^{(\mathrm{vol})}(\omega) \right|^2} \frac{\left| F_{\mathrm{bs}}^{(\mathrm{pred})}(\omega) \right|^2}{V(\omega)}. \tag{18}$$

Similar to the case concerning *TS*, Equations (17) and (18) can involve the use of either a partial- or a full-wave calibration method. Either way, the processing gate of the predictions concerning the calibration sphere must match that used in the calibration measurements (Stanton and Chu, 2008).

Field application

Atlantic herring were studied over Georges Bank off of Cape Cod, MA, in the period 7–15 September 2005, on the "Delaware II". A pelagic trawl was used to sample the fish, and a Simrad EK500 narrowband echosounder, mounted on the hull, was used in observing the distributions of the fish. The towed system was used alternately with the trawl, whereas the hull-mounted echosounder was generally used most of the time. In circumstances in which the hull-mounted system interfered with the towed system, one or more channels of the hull-mounted system were turned off.

Most of the trawl catch was Atlantic herring with a narrow-length distribution, a mean length of 23.6 cm, and a standard deviation of 1.74 cm. Also, as mentioned above, the broadband system on the tow body was calibrated at sea at the site of measurements of the fish, as well as in subsequent calibrations in 2006.

High-resolution acoustic imagery at low frequencies

Through a combination of towing the system near Atlantic herring and using pulse-compression processing, high-resolution images of the fish were obtained (Figures 5 and 6). These images were constructed using data from the medium-frequency channel, 6–17 kHz, which had a range resolution of ~10 cm. Although the beam width at any frequency of this channel is relatively wide, towing near the fish reduced the horizontal footprint of the system. When towing directly over the aggregations of fish (low tens of metres above them), the images were distinctly sharper than the corresponding ones associated with the hull-mounted narrowband system that operated at 120 kHz and had a beam

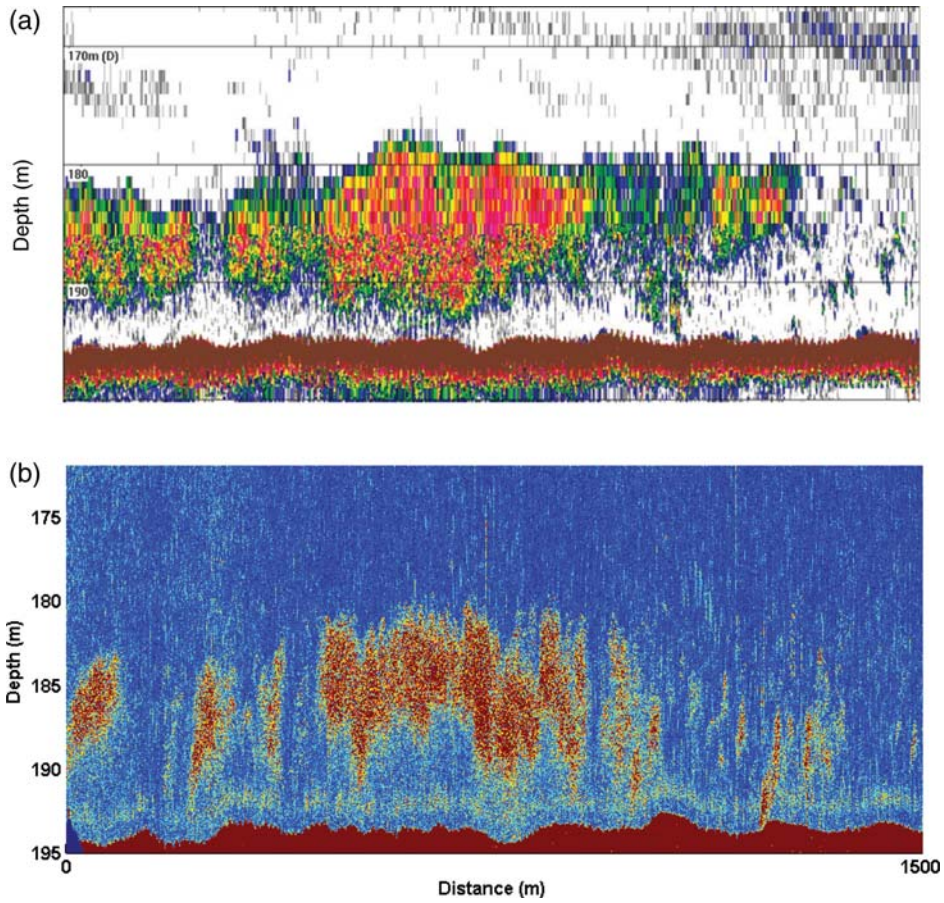

Figure 5. Comparisons of echograms measured using two systems; (a) 120 kHz EK500 narrowband system mounted on the hull of the ship. (b) Compressed-pulse output of broadband medium-frequency system (6–17 kHz) towed near the fish, just above the aggregation. The data from each system were from the same section of water. Both echograms represent volume-backscattering strength on a relative scale. A threshold of −66 dB was imposed on the EK500 data. In (b), the thin layer seen 2 m above the seafloor is an artefact of the system associated with the high echo levels from the seafloor.

width of 7° and a range resolution of ~75 cm (Figure 5). In this example, the contributions to the improvement in resolution over the hull-mounted system by the two methods, towing near the fish and pulse-compression processing, were comparable. Also, when towing the system "through" the fish aggregation, individual fish could be resolved (Figure 6). Again, in contrast, the hull-mounted narrowband system did not resolve these fish.

Another reason for the images to be sharper than the hull-mounted system is that the scattering by the low-frequency system is from the fish only. Scattering from all other types of organism at these frequencies is negligibly small (Figure 1). However, some of the scattering from the high-frequency narrowband system could have been by zooplankton, such as the euphausiids observed in the region. If the distribution of zooplankton was more uniform than the patchy distribution of fish, echoes from the zooplankton could have filled in the spaces between patches of fish in the high-frequency echogram, causing a less distinct image of the patches of fish.

One consequence of towing the system very close to the fish, as in Figure 6, is that the behaviour of the fish may be altered. It is clear from the asymmetrical echotrace of each resolved fish in Figure 6 that fish behaviour was influenced by the presence of the system. Whether this is because of the sound emitted or the compression or movement of the water near the tow body, this phenomenon should be studied more before the system is used for quantitative studies at very close ranges.

Resonance classification and enumeration of fish

A resonance in the low-frequency channel was observed at ~3.7 kHz (Figure 7). This was observed in many sampling windows throughout a patch of Atlantic herring 1 km long and is assumed to be associated with resonance of the swimbladder. This resonance frequency is generally consistent with the resonance observed by Nero *et al.* (2004), although the resonance reported by them was at 2.5 kHz for fish of similar size distribution and at similar depth. The volume-scattering strength shown in Figure 7 was calculated from the compressed-pulse output, using the formulation given in Equation (18). Data are only shown where the channels were most sensitive and the signal-to-noise ratio was acceptable. As a result, there is a gap between the low- and medium-frequency data. Moreover, as described earlier, the data in the 1.7–2.5-kHz band were calibrated, in part, by the seafloor echoes, and are represented by a dashed line.

The echoes showed a resonance at the same frequency throughout all patches (resonance frequencies for a dense and sparse patch are illustrated in Figure 7). This important observation indicates that the volume of the swimbladders, and hence their overall length, is the same throughout the 1.5-km transect. As a result,

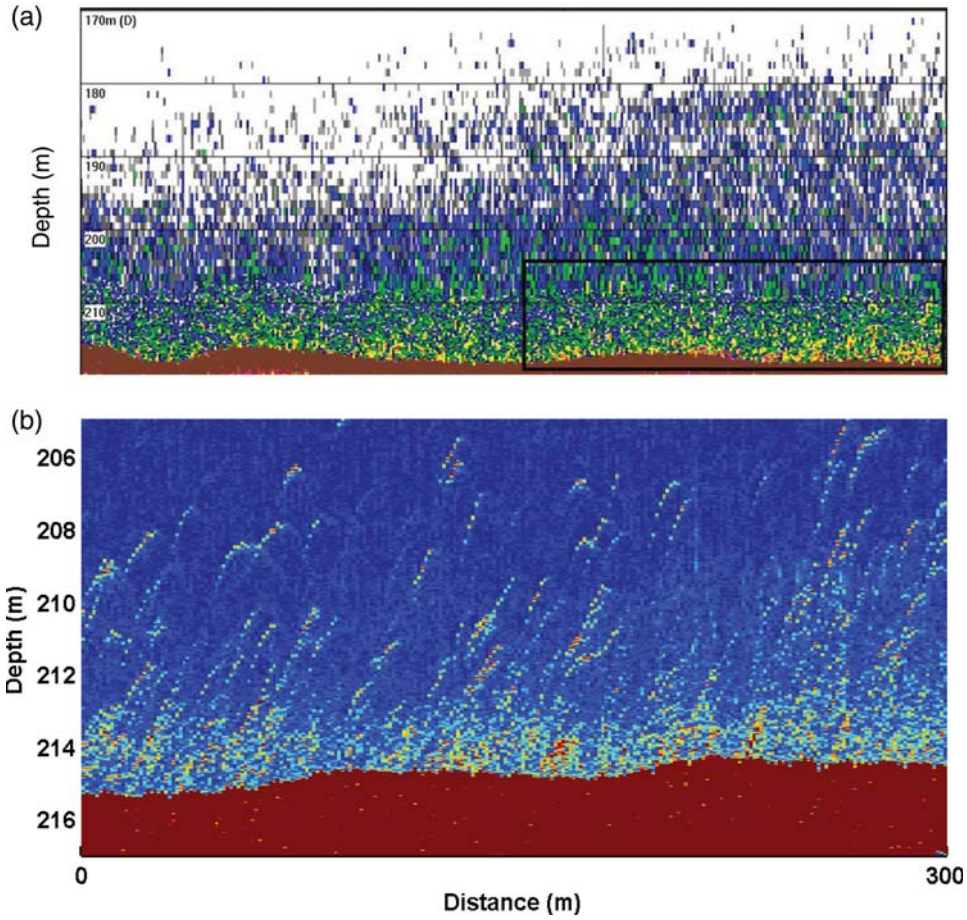

Figure 6. As Figure 5, but with the tow body towed "through" the aggregation of fish. The data collected by the broadband system in (b) correspond to the same section of water outlined in the rectangular section in the lower right corner of the 120-kHz EK500 echogram in (a).

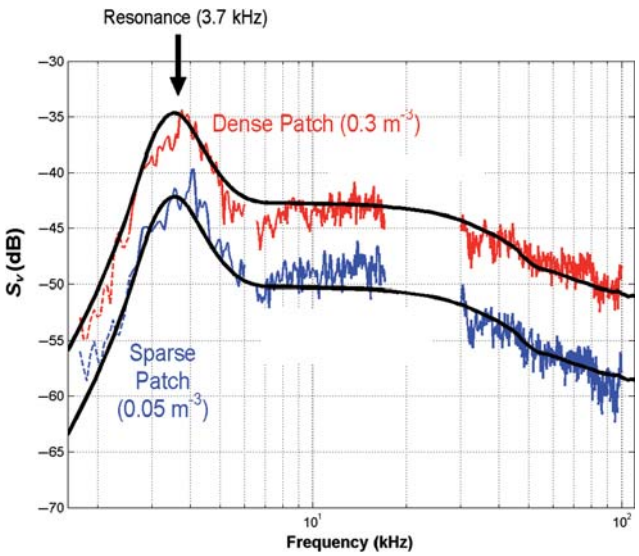

Figure 7. Resonance phenomenon observed in two separate patches of fish. The dense patch is from within the large patch shown in the middle of Figure 5, and the sparse patch is from one of the small patches nearby. The three segments of data correspond to the three broadband acoustic channels. The solid line is a theoretical scattering model.

one can conclude that a change in scattering strength between two portions of the patch is a result of a change in numerical density rather than a change in the size of the fish. As the wavelengths are so long at these frequencies, differences in orientation distribution will not alter the echo level significantly. With this knowledge, therefore, the numerical density of the fish can be estimated.

Using a scattering model developed by Chu *et al.* (2006) and summarized below for the *TS* of fish with swimbladders (the solid curves in Figure 7), the volume-scattering strength can be converted directly to the numerical density of the fish (Figure 8). Here, the density is determined to be as high as 2 per m^3 in the densest portions.

Finally, it is possible, in principle, to determine the spectrum of the scattering from the individual fish in data such as shown in Figure 6. As this is a single-beam system, the individual echoes are convolved with the beam pattern. The beam-pattern effects can be removed from data analytically through the use of, for example, a deconvolution method as initially described by Clay (1983) and refined and summarized by Stanton and Clay (1986).

Scattering model for fish with swimbladders

The Chu *et al.* (2006) model, a hybrid of models for two different frequency regimes, is conceptually similar to the Kirchhoff–Ray–Mode (KRM) model in that in the resonance frequency region, a model is used to describe the swimbladder resonance, and at

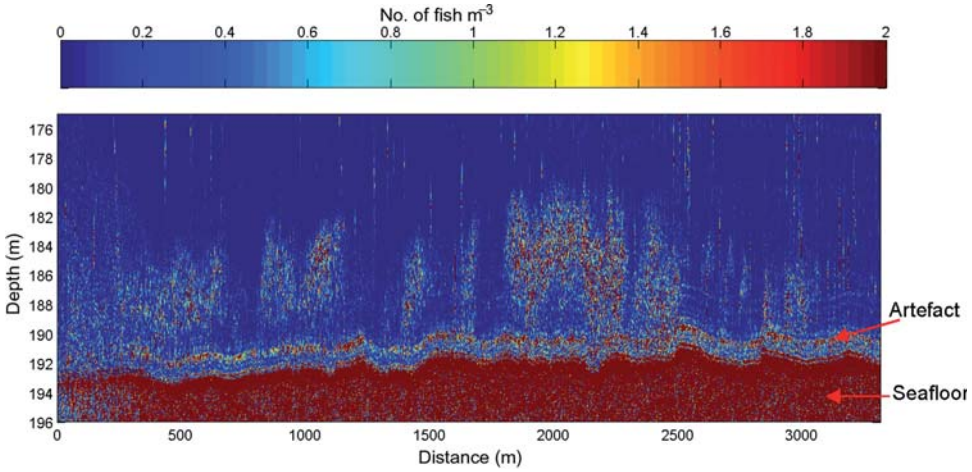

Figure 8. Numerical density of Atlantic herring as determined through resonance classification using the low-frequency acoustic channel. Data are from same transect as in Figure 5, but over a greater distance. There is an artefact in the data, just above the seafloor, associated with the high echo level from the seafloor.

higher frequencies, a model is used to describe geometrical (non-resonant) scattering effects by the swimbladder, such as those associated with orientation (Clay, 1991, 1992; Clay and Horne, 1994; Chu *et al.*, 2006). In addition, and as with the KRM, scattering by fish flesh across all frequencies was accounted for with a third model. Specifically, for frequencies <6 kHz, the resonance-scattering model for gaseous prolate spheroids developed by Ye (1997) was used to describe the scattering by the swimbladder with modifications to include viscous and thermal damping (Love, 1978). For the higher frequencies, the modal-series-based deformed cylinder solution, evaluated for prolate spheroids, was used to describe the scattering by the swimbladder (Stanton, 1989). For all frequencies, the Distorted Wave Born Approximation (DWBA) was used to describe the weakly scattering fish flesh (prolate-spheroid shape). Each of these three models is more accurate than the corresponding models used in the KRM. At any given frequency, the two models (corresponding to the swimbladder and the flesh) were added incoherently (i.e. adding energy). The modal series was converged for the scattering predictions to account for the high-frequency effects. The transition frequency of 6 kHz was chosen for this particular problem where the resonance frequency was at 3.7 kHz, but generally is chosen at the beginning of the flat shoulder at frequencies above the resonance frequency. A smoothing function was used to connect the two models at 6 kHz. Inclusion of the scattering by fish flesh had minimal effects on the predictions of scattering.

The length of the swimbladder was chosen to be one-third of the length of the fish. The density and sound speed of the gas in the swimbladder were chosen for the depth of the fish (185 m). The diameter (twice the semi-minor axis) of the swimbladder was determined from the volume of the swimbladder (with fixed length) which was, in turn, determined initially through Boyle's law. However, for the predicted resonance frequency to match the observed resonance frequency for a depth of 185 m, the volume at the surface needed to be 16 cm^3, increased by a factor of 7 over what it would have been according to Boyle's law and an assumption of neutral buoyancy at the sea surface, in a similar manner to the analysis in Nero *et al.* (2004).

For modelling at the higher frequencies, the orientation distribution of the swimbladder was modelled as $N(8.7^\circ, 3^\circ)$. This is based on the fact that (i) the swimbladder is tilted (vertical plane) by $\sim 5^\circ$ relative to the lengthwise axis of the fish body, and (ii) the pitch of the tow body was tilted by 3.7°. The swimming direction and mean tilt-angle of the fish were not known, so the mean tilt-angle of the fish was assumed to be zero, and the simple sum of the swimbladder angle (5°) and tow-body angle (3.7°) was used as the mean tilt-angle of the swimbladder relative to the incident beam. Also, the standard deviation of 3° was used based on a best fit to the data. The solid black curves in Figure 7 are based on averages over the measured size distribution of the herring and presumed tilt-angle distribution of the swimbladder relative to the incident beam. As the size distribution was so narrow ($\sim$7%), the resonance peak in corresponding curves for single fish had a similar shape to the curves illustrated, but slightly narrower (i.e. with a higher-quality factor).

A major assumption of the modelling is that the sole source of scattering was due to the herring observed in the area. There is significant evidence that that is a reasonable assumption. For example, tight aggregations of fish in this area and near the seafloor are well known to be nearly 100% herring (vs. dispersed aggregations which can contain a significant mix of species). Furthermore, the area was sampled with nets near the time of the acoustic sampling to confirm the composition of fish. However, as there were other fish present in the area, the net sampling was not done simultaneously with the acoustic sampling, and there can be avoidance of the nets by fish, it cannot be known with 100% certainty that the fish were all herring. Therefore, the need to adjust the volume of the swimbladder in a similar manner as in the Nero *et al.* (2004) analysis is based on the same assumption that only herring contributed to the resonance observed.

Daylight surface swarms of small scatterers

Scatterers other than fish with swimbladders were also observed with the system (Figure 9). Near the sea surface, compact aggregations of scatterers were observed with the high-frequency channel. The measured scattering strength increased rapidly and monotonically with frequency over most of the band. Comparison with a fluid cylinder scattering model shows that most of this region varies with the fourth power of frequency, consistent with

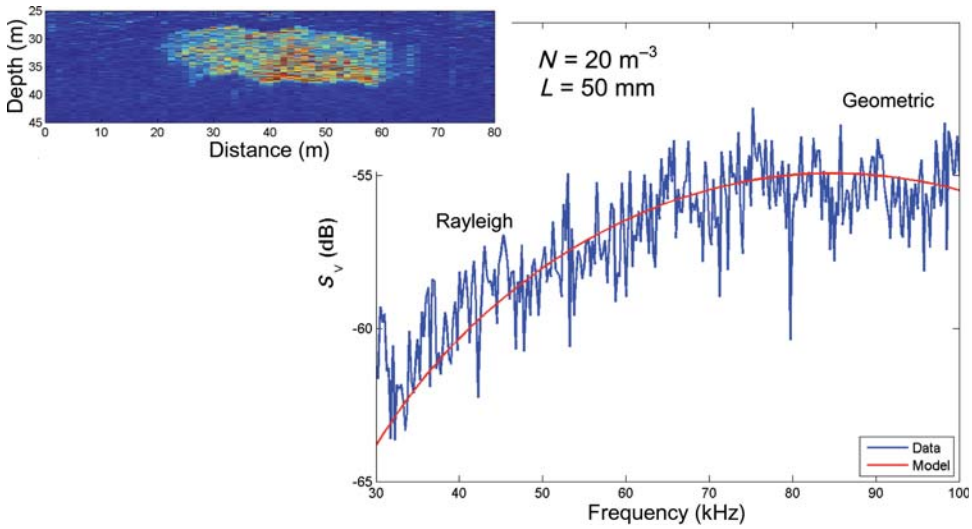

Figure 9. Acoustic data from a near-surface daylight swarm of what appears to be zooplankton ~5 cm long. The transition from Rayleigh to geometric scattering is at ~85 kHz.

Rayleigh scattering. The frequency at which the curve transitions from Rayleigh to geometric scattering is ~85 kHz, consistent with elongated fluid-like scatterers ~5 cm long. Using that length in the scattering model in combination with measured volume-scattering strength, the numerical density of the organisms is estimated to be 20 per m^3. Although these aggregations were not sampled directly with nets, their shape and occurrence (in daylight near the surface) are consistent with swarming behaviour associated with the reaction of euphausiids to prey (Nicol, 1986).

Conclusions

A broadband commercial system was adapted for studying fish. With the wide range of frequencies, there were significant improvements over conventional narrowband systems.

(i) *Improvement in resolution*. Through the use of pulse-compression processing, the temporal resolution was improved to bring it comparable with the limit of the inverse bandwidth. As a result, the range resolutions were ~20, 10, and 3 cm for the 1.7–10, 6–17, and 30–100-kHz channels. The lateral resolution was also improved by towing close to the fish, although it was demonstrated that the system should not be towed too close, or the behaviour of the fish would be altered. As a result of the improvement in resolution, the patchiness of the fish was better quantified, individual fish could be resolved, and fish near the seafloor could be distinguished from the seafloor.

(ii) *Resonance classification*. With the low-frequency channel extending down to 1.7 kHz, the resonance frequency of Atlantic herring was observed, providing accurate estimates of size and density of fish.

(iii) *Spectral discrimination*. Because of the nearly continuous coverage of a wide range of frequencies, there was improved ability over single- or multifrequency narrowband echosounders to discriminate between different types of organisms—fish with swimbladders and zooplankton in this case.

(iv) *Reductions in ambiguities*. Detection of fish at the low kilohertz frequencies eliminates the possibility that the echoes may have been from zooplankton. Moreover, at these low frequencies, the echoes are not sensitive to orientation distribution. As the resonance frequency was observed to be the same across the aggregation of fish studied, any changes in echo level can be attributed definitively to changes in the numerical density of the fish. The strength of this last statement is in sharp contrast to interpretation of data from traditional high-frequency echosounders, where changes in echo levels can be attributed to changes in numerical density, type, or size of fish, their orientation distribution, or some combination. Here, the uncertainties are eliminated, and the only remaining cause for changes in echo level is density of the fish.

Another important broad accomplishment presented here is the fact that the improvements were made possible through adaptation of a commercially available system. Subsets of the improvements have been accomplished by previous investigators through the use of conventional or prototype systems. However, these desired capabilities are now available through the modification of a commercial system for routine use.

New methods for calibrating single-beam broadband systems were also developed. The key aspect to the advance was in the elimination of the influence of the resonances of the calibration sphere that would otherwise appear in the broadband echo. This was achieved through a combination of pulse-compression processing of the broadband signals, and a partial-wave scattering analysis of the echoes. Given the complexity of this new and advanced method, the details are given separately in Stanton and Chu (2008) and are both summarized and applied to the ocean study here.

Finally, the equations are derived and presented here for the first time relating *TS* and volume-backscattering strength to quantities associated with broadband processing of echo data.

Acknowledgements

Portions of this paper were published in Stanton *et al.* (2007). We thank the captains and crews of the FRV "Delaware II" and RV

"Tioga", and the following people from the Woods Hole Oceanographic Institution (WHOI), Woods Hole, MA, for their various roles in the research: Jeff Lord, Will Ostrom, Andy Girard, and Shirley Barkley; along with D. Ben Reeder of the Naval Postgraduate School, Monterey, CA, for his participation in the cruise on the "Delaware II", and Steve Wright, Mohammed Sanhaji, and Jason Sara of Edgetech, Boca Raton, FA, for their participation in the design of the new system. The research was supported by the US Office of Naval Research, grants number N00014-04-1-0440 and N00014-04-1-0475, NOAA/CICOR cooperative agreement NA17RJ1223, NOAA/National Marine Fisheries Service, and the J. Seward Johnson Chair of the WHOI Academic Programs Office.

References

Au, W. W. L., and Benoit-Bird, K. J. 2008. Broadband backscatter from individual Hawaiian mesopelagic boundary community animals with implications for spinner dolphin foraging. Journal of the Acoustical Society of America, 123: 2884–2894.

Chapman, R. P., Bluy, O. Z., Adlington, R. H., and Robison, A. E. 1974. Deep scattering layer spectra in the Atlantic and Pacific Oceans and adjacent seas. Journal of the Acoustical Society of America, 56: 1722–1734.

Chapman, R. P., and Marshall, J. R. 1966. Reverberation from deep scattering layers in the western North Atlantic. Journal of the Acoustical Society of America, 40: 405–411.

Chu, D., and Stanton, T. K. 1998. Application of pulse compression techniques to broadband acoustic scattering by live individual zooplankton. Journal of the Acoustical Society of America, 104: 39–55.

Chu, D., Stanton, T. K., Jech, J. M., and Reeder, D. B. 2006. Modeling of the backscattering by swimbladder-bearing fish. Journal of the Acoustical Society of America, 120: 3105.

Clay, C. S. 1983. Deconvolution of the fish scattering PDF from the echo PDF for a single transducer sonar. Journal of the Acoustical Society of America, 73: 1989–1994.

Clay, C. S. 1991. Low-resolution acoustic scattering models: fluid-filled cylinders and fish with swimbladders. Journal of the Acoustical Society of America, 89: 2168–2179.

Clay, C. S. 1992. Composite ray-mode approximations for backscattered sound from gas-filled cylinders and swimbladders. Journal of the Acoustical Society of America, 92: 2173–2180.

Clay, C. S., and Horne, J. K. 1994. Acoustic models of fish: the Atlantic cod (*Gadus morhua*). Journal of the Acoustical Society of America, 96: 1661–1668.

Diachok, O. 2002. Bioacoustic absorption spectroscopy: estimation of the biomass of fish with swimbladders. Bioacoustics, 12: 271–274.

Diachok, O., Liorzou, B., and Scalabrin, C. 2001. Estimation of the number density of fish from resonance absorptivity and echo sounder data. ICES Journal of Marine Science, 58: 137–153.

Ehrenberg, J. E., and Torkelson, T. C. 2000. FM slide (chirp) signals: a technique of significantly improving the signal-to-noise in hydroacoustic assessment systems. Fisheries Research, 47: 193–199.

Hall, M. 1981. Measurements of acoustic volume backscattering in the Indian and Southern Oceans. Australian Journal of Marine Freshwater Research, 32: 855–876.

Hall, M., and Quill, A. F. 1983. Biological sound scattering in an ocean eddy. Australian Journal of Marine Freshwater Research, 34: 563–572.

Hersey, J. B., Backus, R. H., and Hellwig, J. 1962. Sound-scattering spectra of deep scattering layers in the western North Atlantic Ocean. Deep Sea Research, 8: 196–210.

Holliday, D. V. 1972. Resonance structure in echoes from schooled pelagic fish. Journal of the Acoustical Society of America, 51: 1322–1332.

Lee, W-J., Stanton, T. K., and Lavery, A. C. 2009. Broadband acoustic backscattering from live squid: experiment and analysis. Journal of the Acoustical Society of America, 125: 2550.

Love, R. H. 1978. Resonant acoustic scattering by swimbladder-bearing fish. Journal of the Acoustical Society of America, 64: 571–580.

Løvik, A., and Hovem, J. M. 1979. An experimental investigation of swimbladder resonance in fishes. Journal of the Acoustical Society of America, 66: 850–854.

Medwin, H., and Clay, C. S. 1998. Fundamentals of Acoustic Oceanography. Academic Press, Boston.

Nero, R. W., Thompson, C. H., and Jech, J. M. 2004. *In situ* acoustic estimates of the swimbladder volume of Atlantic herring (*Clupea harengus*). ICES Journal of Marine Science, 61: 323–337.

Nicol, S. 1986. Shape, size and density of daytime surface swarms of the euphausiid *Meganyctiphanes norvegica* in the Bay of Fundy. Journal of Plankton Research, 8: 29–39.

Reeder, D. B., Jech, J. M., and Stanton, T. K. 2004. Broadband acoustic backscatter and high-resolution morphology of fish: measurement and modeling. Journal of the Acoustical Society of America, 116: 747–761.

Ross, T., and Lawson, G. 2009. Long-term broadband acoustic observations of zooplankton scattering layers in Saanich Inlet, British Columbia. Journal of the Acoustical Society of America, 125: 2551.

Sand, O., and Hawkins, A. D. 1973. Acoustic properties of the cod swimbladder. Journal of Experimental Biology, 58: 797–820.

Stanton, T. K. 1989. Sound scattering by cylinders of finite length. 3, Deformed cylinders. Journal of the Acoustical Society of America, 86: 691–705.

Stanton, T. K., and Chu, D. 2008. Calibration of broadband active acoustic systems using a single standard spherical target. Journal of the Acoustical Society of America, 124: 128–136.

Stanton, T. K., Chu, D., Jech, J. M., and Irish, J. D. 2007. A broadband echosounder for resonance classification of swimbladder-bearing fish. Proceedings of the 2007 IEEE Oceans 07 Conference, Aberdeen. 3 pp.

Stanton, T. K., and Clay, C. S. 1986. Sonar echo statistics as a remote sensing tool: volume and sea floor. IEEE Journal of Oceanic Engineering, OE-11: 79–96.

Stanton, T. K., Reeder, D. B., and Jech, J. M. 2003. Inferring fish orientation from broadband-acoustic echoes. ICES Journal of Marine Science, 60: 524–531.

Sundnes, G., and Sand, O. 1975. Studies of a physostome swimbladder by resonance frequency analyses. Journal du Conseil International pour l'Exploration de la Mer, 36: 176–182.

Thompson, C. H., and Love, R. H. 1996. Determination of fish size distributions and areal densities using broadband low-frequency measurements. ICES Journal of Marine Science, 53: 197–201.

Turin, G. L. 1960. An introduction to matched filters. Institute of Radio Engineers Transactions on Information Theory, IT-6: 311–329.

Weston, D. 1967. Sound propagation in the presence of bladder fish. *In* Underwater Acoustics, pp. 55–58. Ed. by V. Albers. Plenum Press, New York.

Ye, Z. 1997. Low-frequency acoustic scattering by gas-filled prolate spheroids in liquids. Journal of the Acoustical Society of America, 101: 1945–1952.

doi:10.1093/icesjms/fsp262